A novel combined estimation method of online full-parameter identification and adaptive unscented particle filter for Li-ion batteries SOC based on fractional-order modeling.

CHEN, L., WANG, S., JIANG, H., FERNANDEZ, C. and XIONG, X.

2021

INTERNATIONAL JOURNAL OF
ENERGY RESEARCH

A novel combined estimation method of online full-parameter identification and adaptive unscented particle filter for Li-ion batteries SOC based on fractional-order modeling

Journal:	*International Journal of Energy Research*
Manuscript ID	ER-21-19458.R1
Wiley - Manuscript type:	Research Article
Date Submitted by the Author:	17-Apr-2021
Complete List of Authors:	Chen, Lei Wang, Shunli; Southwest University of Science and Technology, School of Information Engineering Jiang, Hong Fernandez, Carlos; Robert Gordon University Xiong, Xin; Southwest University of Science and Technology, School of Information Engineering
Keywords:	Li-ion battery, Improve fractional equivalent circuit model, Full-parameter identification, State of charge, Adaptive fractional-order unscented particle filter

A novel combined estimation method of online full-parameter identification and adaptive unscented particle filter for Li-ion batteries SOC based on fractional-order modeling

Lei Chen[a], Shunli Wang[a,*], Hong Jiang[a], Carlos Fernandez[b], Xin Xiong[a]

[a]*School of Information Engineering, Southwest University of Science and Technology, Mianyang 621010, China;*

[b]*School of Pharmacy and Life Sciences, Robert Gordon University, Aberdeen AB10-7GJ, UK.*

Abstract: Accurate estimation of the state of charge (SOC) of Li-ion battery can ensure the reliability of the storage system. A combined estimator of online full-parameter identification and adaptive unscented particle filter for Li-ion battery SOC based on an improved fractional-order model is proposed, which overcomes the shortcomings of the traditional SOC cumulative error and the difficulty of OCV acquisition. The proposed adaptive fractional unscented particle filter algorithm introduces fractional parameters as hidden parameters and reduces the complexity of the algorithm iteration by reducing the number of particles. At the same time, the noise adaptive algorithm based on the residual sequence can solve the divergence problem of the filter and improve the adaptability of the algorithm. To verify the feasibility of the algorithm under complex operating conditions, the urban dynamometer driving schedule dynamic working conditions of Li-ion batteries are verified. The experimental results show that the evaluation index of the algorithm is the best, the RMSE is 0.67%, and the SOC estimation is more accurate. It shows that the algorithm has strong robustness and fast convergence.

Key words: Li-ion battery; Improve fractional-order equivalent circuit model; Full-parameter identification; State of charge; Adaptive fractional-order unscented particle filter;

***Corresponding author**: Shun-Li Wang. Tel: +86-15884655563. E-mail address: 497420789@qq.com.

1. Introduction

With the breakthrough of energy storage technology, the global energy structure dominated by traditional energy is undergoing revolutionary changes [1]. Li-ion batteries are widely used in the fields of power supply, high-efficiency energy storage and backup power supply due to their high energy density, long cycle life, safety and pollution-free advantages, and become one of the effective ways to solve the problem of electrical energy storage [2]. Li-ion batteries are used as energy storage components to realize the conversion of chemical energy and electric energy through chemical reactions [3]. Battery management system (BMS) can monitor the performance of the battery in real-time to prevent the irreversible effects of over-charge and over-discharge on battery life. However, there are problems of inaccurate remaining time prediction caused by imperfect state estimation[4], as well as potential safety hazards such as thermal management [5] and energy imbalance [6]. Since SOC cannot be directly measured in practical applications, how to explore new battery modeling methods and state estimation methods has become the focus of attention in academics and industry [7].

Accurate modeling of Li-ion batteries is an indispensable part of BMS, and it is also the basis of accurate estimating of battery SOC [8]. The equivalent circuit model (ECM) is currently the most widely used. [9]. Because the battery voltage changes rapidly at the beginning and end of charging and discharging, it is difficult

to accurately simulate the strong nonlinearity of the battery through ECM. In n-order RC, ECMs can improve their accuracy by increasing the number of RC network modules, but this will make the model structure more complex, greatly increase the amount of calculation, and bring difficulties to model parameter identification and practical applications [10]. Due to the strong fractional characteristic of the capacitors, some researchers have begun to pay attention to the application of fractional capacitors in battery modeling [11, 12]. Hu et al. [13] introduced the constant phase element (CPE) from the perspective of the frequency domain, which proved that the fractional-order model (FOM) of power battery based on fractional calculus theory is more accurate. Jin et al. [14] compared the SOC estimation accuracy of dual polarization model (DPM) and FOM under different working conditions, and demonstrated the estimation error based on FOM is always less than that of DPM.

Since the FOM has higher accuracy than the integer-order model (IOM) in theory, some scholars have begun to study the SOC estimation algorithm based on FOM [15, 16]. In ref. [17], Xu et al. proposed two FOMs-based dual Kalman filter (DKF) and dual extended Kalman filter (DEKF) methods to estimate the accuracy of the SOC, which proved the robustness and adaptability of the algorithm, but there is a linear cut-off error. In ref. [18], Tian et al. measured the SOC estimation performance under different temperature and aging conditions based on fractional-order unscented Kalman filter (FOUKF), which verified the accuracy of the model and the effectiveness of the estimation method. However, these two algorithms are usually limited to Gaussian distribution [19, 20]. Particle filtering (PF) has unique advantages in processing nonlinear systems that are not constrained by assumptions such as noise and models and are gradually becoming a research hotspot [21-25]. Nevertheless, there are few PF algorithms based on FOM [26-28]. Li et al. [29] introduced the FOM combined with the PF method for SOC estimation, without considering the large SOC estimation error caused by insufficient particle diversity and scarcity in the PF algorithm. Wang et al. [30] proposed a SOC estimation method that combined PF and fractional-order extended Kalman filter (FOEKF), which has better accuracy and fractional real-time performance, but the computational complexity is relatively high.

Most of the aforementioned documents based on FOMs use offline identification methods [31, 32]. Few documents consider online real-time estimation of FOM parameters [33, 34]. Due to the introduction of fractional calculus, how to determine the differential order α and realize the online identification of other parameters is a technical difficulty [35-37]. The existing literature lacks research and analysis on the online joint estimation of fractional parameters and SOC. Although the SOC estimation method proposed in [38] takes into account the fractional characteristics of the battery and had a high estimation accuracy, it did not consider the influence of noise interference [39, 40]. Therefore, a combined estimator of online full-parameter identification and adaptive unscented particle filter for Li-ion battery SOC based on an improved FOM is proposed, which not only solves the shortcomings of the PF algorithm but also solves the problem of filter divergence and improves the adaptability of the algorithm. Furthermore, the closed-loop estimation formed by online full-parameters identification and SOC combined estimation can significantly improve the accuracy of SOC.

2. Mathematical analysis

2.1. Fractional calculus

The Grünwald-Letnikov (G-L) definition can directly discretize the fractional differential equation, as shown in Eq. (1). Through the transformation relationship of the above Equation, the application field of fractional calculus defined by G-L can be extended from a positive integer field to a real number field.

$$D_t^a f(t) = \lim_{h\to 0} h^{-a} \sum_{j=0}^{[(t-t_0)/h]} (-1)^j \binom{a}{j} f(t-jh) \quad (1)$$

Where $D_t^a f(t)$ represents a first-order differential of $f(t)$, α represents the differential order, h is the sampling period, $\omega_j^a = (-1)j\binom{a}{j}$ indicates the weighted coefficients, the Newton binomial coefficient $\binom{a}{j}$ can be expressed as shown in Eq. (2).

$$\binom{a}{j} = \begin{cases} 1 & j = 0 \\ \dfrac{\text{a(a-1)...(a-j+1)}}{j!} & j > 0 \end{cases} \quad (2)$$

2.2. Equivalent modeling

To overcome the shortcomings of traditional OCV acquisition difficulties， the ideal voltage source of FOM is regarded as a controlled current source related to SOC, and the relationship between the controlled current source and SOC is related to SOC-OCV. OCV is a dynamic parameter that changes with time, so the proposed model has high accuracy during the whole cycle of the battery. The improved FOM is shown in Fig 1. As a bridge between the two parts, the nonlinear relationship between OCV and SOC is critical in BMS because it is an important way to calibrate the Ampere-hour (Ah) integral method.

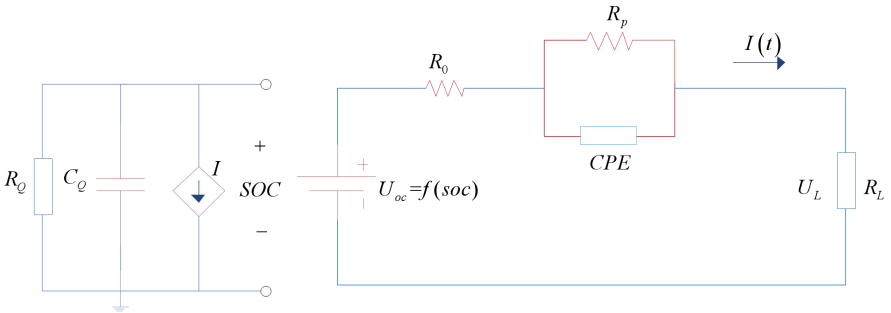

Fig1. Runtime-based fractional-order battery model

The model consists of a run-time circuit and FOM, the left part contains a capacitor C_Q represents the battery available capacity, a self-discharge resistor R_Q, and a current control current source I. The right part of the model is similar to the Thevenin model, where R_0 is the internal resistance, R_p is the polarization resistance, and CPE is a constant phase element, whose fractional order is denoted as α. U_L is terminal voltage, U_{OC} is the open-circuit voltage, which is a function of SOC, defined in Eq. (3). K_0, K_1, K_2, K_3, and K_4 are the undetermined coefficients.

$$U_{OC} = K_0 - K_1 SOC(k) - K_2 / SOC(k) + K_3 \ln\left(SOC\left(k\right)\right) + K_4 \ln\left(1 - SOC\left(k\right)\right) \quad (3)$$

The mathematical derivation of the battery model is shown in Eq. (4). C_Q is defined as a function of the

nominal capacity Q_{nom} of the battery, f_1 (*Cycle*) and f_2 (*Temp*) are defined as correction coefficients for battery cycle life and temperature. The influence of temperature and cycle life on battery capacity is ignored.

$$C_Q = 3600.Q_{nom}.f_1(Cycle).f_2(Temp) \quad (4)$$

CPE has an attribute between resistance and capacitance, as shown in Eq. (5), Where C_1 is the impedance coefficient.

$$Z_{CPE} = \frac{1}{C_1 S^a} \quad (5)$$

The differential expression of the SOC expression is defined as shown in Eq. (6), η represents the charge-discharge current ratio.

$$D^1 SOC(t) = -\frac{\eta I(t)}{3600 C_Q} \quad (6)$$

According to Kirchhoff's law, the voltage can be expressed as shown in Eq. (7). The second equation is a differential equation for the parallel circuit voltage.

$$\begin{cases} U_L = U_{oc}(SOC) + U_0 + U_p \\ D^a U_p = \dfrac{I}{C_1} - \dfrac{U_p}{R_p C_1} \end{cases} \quad (7)$$

Using the definition of G-L, the state space equation is discretized, and the discretized state space equation is obtained as shown in Eq. (8).

$$\begin{cases} \begin{bmatrix} SOC(k) \\ U_p(k) \end{bmatrix} = \begin{bmatrix} 0 & 1 \\ -\dfrac{T^a}{R_p C_1} & 0 \end{bmatrix} \begin{bmatrix} SOC(k-1) \\ U_p(k-1) \end{bmatrix} + \begin{bmatrix} \dfrac{\eta T}{C_Q} \\ \dfrac{T^a}{C_1} \end{bmatrix} I_{k-1} - \begin{bmatrix} 0 \\ \sum_{j=1}^{k} \omega_j^a U_p(k-j) \end{bmatrix} + \omega_{k-1} \\ U_L(k) = U_{OC}(SOC) - [0 \quad 1][SOC(k) \quad U_p(k)]^T - R_0 I_k + v_{k-1} \\ U_{OC} = K_0 - K_1 SOC(k) - K_2 / SOC(k) + K_3 \ln(SOC(k)) + K_4 \ln(1 - SOC(k)) \end{cases} \quad (8)$$

2.3. Parameter identification

The particle swarm optimization algorithm is used to obtain the differential order α, and the remaining parameters are identified based on the forgetting factor recursive least square method. The impedance transfer function of FOM is defined as shown in Eq. (9).

$$\frac{U_{OC}(s) - U_L(s)}{I(s)} = \frac{R_p}{R_p C_1 s^a + 1} + R_0 \quad (9)$$

Based on G-L, the above equation can be discretized as shown in Eq. (10).

$$y(t) + R_p C_1 T^{-a} \sum_{i=0}^{N} (-1)^i \binom{a}{i} y(t - iT) = I(t)(R_0 + R_p) + R_0 R_p C_1 T^{-a} \sum_{i=0}^{N} (-1)^i \binom{a}{i} I(t - iT) \quad (10)$$

The memory length is truncated and converted to a first-order difference equation, as shown in Eq. (11).

$$y(k) = -\omega_1^a \frac{m}{T^a + m} y(k-1) + \left(\frac{T^a R_p}{T^a + m} + R_0\right) I(k) + \omega_1^a \frac{m R_0}{T^a + m} I(k-1) \quad (11)$$

The optimal estimated parameters can be obtained through FFRLS as shown in Eq. (12).

$$\begin{cases} K(k) = P(k\text{-}1)\phi(k)[\phi^T(\mathrm{k})P(k\text{-}1)\phi(k) + \lambda]^{-1} \\ P(k) = \lambda^{-1}[I - K(k)\phi^T(k)]P(k\text{-}1) \\ e(k) = y(k) - \phi^T(\mathrm{k})\hat{\theta}(k\text{-}1) \\ \hat{\theta}(k) = \hat{\theta}(k\text{-}1) + K(k)e(k) \end{cases} \quad \text{.....(12)}$$

The parameters values to be identified are further obtained shown in Eq. (13).

$$\begin{cases} R_0 = a_3 / a_1 \\ m = a_1 T^a / (a - a_1) \\ R_p = (a_2 - R_0)(T^a + m)/T^a \\ C_1 = m / R_p \end{cases} \quad \text{.....(13)}$$

According to the bilinear change, the full-parameter identification formula is obtained as shown in Eq. (14).

$$U_{L,k} = (1-a_1)(K_0 - K_1 SOC_k - K_2 / SOC_k + K_3 \ln(SOC_k) + K_4 \ln(1-SOC_k)) + a_1 U_{L,k-1} + a_2 I_k + a_3 I_{k-1}. \quad \text{.....(14)}$$

Define φ_k as the known input and output vectors are shown in Eq. (15), θ_k are the parameters to be undetermined shown in Eq. (16).

$$\varphi_k = \begin{bmatrix} 1 & -SOC_k & -1/SOC_k & \ln SOC_k & \ln(1-SOC_k) & U_{L,k-1} & I_{L,k} & I_{L,k-1} \end{bmatrix} \text{.....(15)}$$

$$\theta_k = \begin{bmatrix} (1-a_1)k_0 & (1-a_1)k_1 & (1-a_1)k_2 & (1-a_1)k_3 & (1-a_1)k_4 & a_1 & a_2 & a_3 \end{bmatrix} \text{.....(16)}$$

The implementation process of full-parameter identification based on FFRLS is shown in Tab 1.

Tab 1 Model full-parameter identification process based on FFRLS

(1) Parameter identification of OCV model	(2) Parameter identification of battery model
(a) Initialization	(a) Initialization
$\begin{cases} \varphi_{1,k\|k=0} = \begin{bmatrix} 1 & -SOC_0 & -1/SOC_0 & \ln SOC_0 & \ln(1-SOC_0) \end{bmatrix} \\ \theta_{1,k\|k=0} = \begin{bmatrix} (1-a_1)k_0 & (1-a_1)k_1 & (1-a_1)k_2 & (1-a_1)k_3 & (1-a_1)k_4 \end{bmatrix} \end{cases}$	$\begin{cases} \varphi_{2,k\|k=1} = \begin{bmatrix} (U_{L,1} - U_{OC,1}) & i_1 & i_0 \end{bmatrix} \\ \theta_{2,k\|k=1} = \begin{bmatrix} a_1 & a_2 & a_3 \end{bmatrix} \end{cases}$
(b) Calculate gain $K_{1,k}$ and error covariance matrix $P_{1,k}$	(b) Calculate gain $K_{2,k}$ and error covariance matrix $P_{2,k}$
$\begin{cases} K_{1,k} = P_{1,k-1}\varphi_{1,k}[\varphi_{1,k}^T P_{1,k-1}\varphi_{1,k} + \lambda_1]^{-1} \\ P_{1,k} = \lambda_1^{-1}[I - K_{1,k}\varphi_{1,k}^T]P_{1,k-1} \end{cases}$	$\begin{cases} K_{2,k} = P_{2,k-1}\varphi_{2,k}[\varphi_{2,k}^T P_{2,k-1}\varphi_{2,k} + \lambda_2]^{-1} \\ P_{2,k} = \lambda_2^{-1}[I - K_{2,k}\varphi_{2,k}^T]P_{2,k-1} \end{cases}$
(c) Calculate the error $e_{1,k}$ and update model parameter $\hat{\theta}_{1,k}$	(c) Calculate the error $e_{2,k}$ and update model parameter $\hat{\theta}_{2,k}$
$\begin{cases} e_{1,k} = y_{1,k} - \varphi_{1,k}^T \hat{\theta}_{1,k-1} \\ \hat{\theta}_{1,k} = \hat{\theta}_{1,k-1} + K_{1,k} e_{1,k} \end{cases}$	$\begin{cases} e_{2,k} = y_{2,k} - \varphi_{2,k}^T \hat{\theta}_{2,k-1} \\ \hat{\theta}_{2,k} = \hat{\theta}_{2,k-1} + K_{2,k} e_{2,k} \end{cases}$
(d) Update the predicted $U_{oc,k}$	(d) Update the predicted $U_{L,k}$
$U_{oc,k} = \varphi_{1,k}\hat{\theta}_{1,k}$	$U_{L,k} = \varphi_{2,k}\hat{\theta}_{2,k}$

3. Adaptive fractional-order unscented particle filter algorithm

3.1 Adaptive fractional-order unscented Kalman filter algorithm

FOUKF is a filtering algorithm based on unscented transformation. In the process of state update and measurement update, the UT transformation uses sampling points to approximate the probability distribution of state variables and completes the transfer of the statistical mean and covariance of random variables. The sample points of FOUKF include the memory effect of FOM on past time. The optimal estimation of the last state is added for time update and prior estimation so that the state vector contains the statistical information of the past time. Therefore, compared with UKF, FOUKF can estimate the battery status more accurately. Fig.2 shows the flow chart of SOC estimation based on AFOUKF.

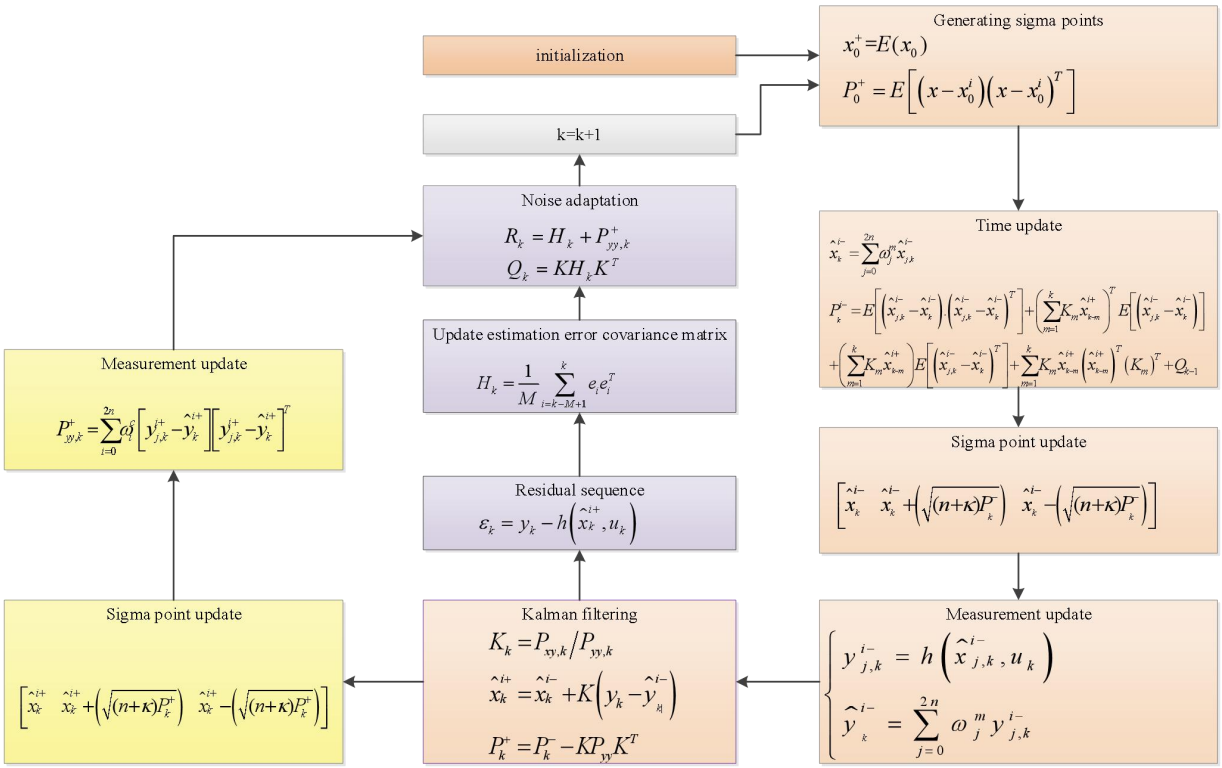

Fig 2 The flow chart of SOC estimation based on residual sequence adaptive fractional-order unscented Kalman filter

The accuracy of the KF method depends on the reliable process noise and measurement noise. To obtain accurate state estimation, the residual-based covariance matching technique is applied to monitor and track the changes of noise, and the parameters are adjusted adaptively to maintain the accuracy of the state estimation. The residual sequence is defined as the difference between the input measurement and the posterior estimation measurement, as shown in Eq. (17). The covariance matrix of the residual sequence is shown in Eq. (18).

$$\varepsilon_k = y_k - h\left(\hat{x}_k^{i+}, u_k\right) \quad \text{.....(17)}$$

$$H_k = \frac{1}{M}\sum_{i=k-M+1}^{k} \varepsilon_i \varepsilon_i^T \quad \text{.....(18)}$$

The measurement error covariance matrix and the process error covariance matrix are obtained as shown in Eq.

(19), which ensures the positive definiteness of the matrix and solves the filtering divergence problem.

$$R_k = H_k + P_{yy,k}^{+}$$
$$Q_k = KH_kK^T \quad \text{..... (19)}$$

3.2 Adaptive fractional-order unscented particle filter algorithm

The noise distribution of the FOUKF algorithm must satisfy the Gaussian distribution. The particle filter is a non-parametric estimation method based on Monte Carlo and Bayesian estimation, which breaks the noise restriction of Gaussian distribution. However, its huge computing burden is still the main obstacle to practical applications. Moreover, system performance degradation and sample exhaustion are the main problems of the basic sequential importance sampling-resampling particle filter algorithm. An adaptive fractional unscented particle filter (AFOUPF) is proposed to overcome the shortcomings of the PF algorithm. AFOUPF is a UPF algorithm composed of PF and FOUKF. The flow chart of SOC estimation based on AFOUPF is shown in Fig.3.

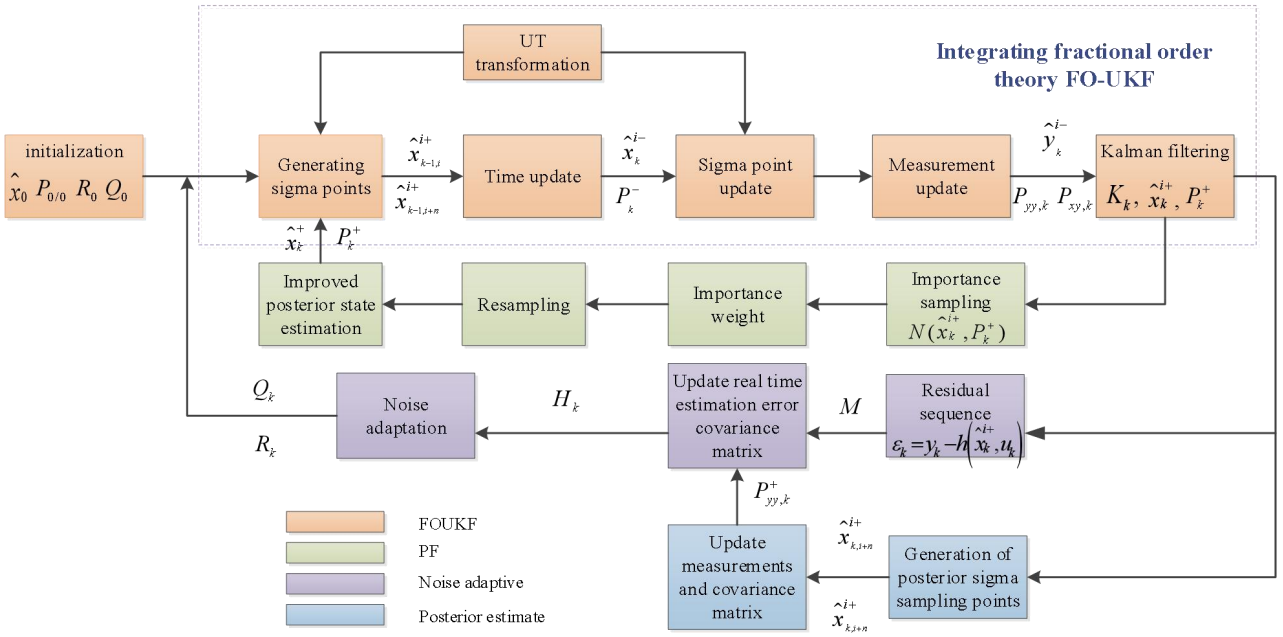

Fig 3 The flow chart of the adaptive fractional-order unscented particle filter algorithm

According to the discrete state-space equation of the FOM, the AFOUPF algorithm is used to estimate the SOC. The AFOUPF algorithm uses UKF to introduce fractional calculus theory to update each particle in the iteration process and uses the mean value and covariance of the obtained particles to update the new particles in the next sample, which is closer to the true posterior probability density distribution. The fractional-order parameters after importance sampling are included as hidden parameters, which can reduce the number of particles required while obtaining the same estimation accuracy. The summary of the AFOUPF algorithm is shown in Tab.2.

Tab 2 The summary of the AFOUPF algorithm

The discrete state-space equation of FOM

$$x_k = Ax_{k-1} + BI_{k-1} - \sum_{j=1}^{k} K_j x_{k-j} + \omega_{k-1}$$

$$y_k = Cx_k + DI_k + \upsilon_k$$

Step 1: Initialization

$$x_0^+ = E(x_0)$$

$$P_0^+ = E\left[\left(x - x_0^j\right)\left(x - x_0^j\right)^T\right]$$

Step 2: Time update

(a) Compute sigma points

$$\hat{x}_{k-1}^{i+} = \left[\hat{x}_{k-1}^+ \quad \hat{x}_{k-1}^+ + \left(\sqrt{(n+\kappa)P_{k-1}^+}\right) \quad \hat{x}_{k-1}^+ - \left(\sqrt{(n+\kappa)P_{k-1}^+}\right)\right]$$

(b) Compute weights

$$\begin{cases} \omega_0^m = \dfrac{\lambda}{n+\lambda} \\ \omega_0^c = \dfrac{\lambda}{n+\lambda} + 1 - \alpha^2 + \beta \\ \omega_i^m = \omega_i^c = \dfrac{1}{2(n+\lambda)}, \quad i = 1...2n \end{cases}$$

(c) Prior state estimation

$$\hat{x}_{j,k}^{i-} = f\left(\hat{x}_{k-L-1:k-1}^{i+}, u_{k-1}\right)$$

$$\hat{x}_k^{i-} = \sum_{j=0}^{2n} \omega_j^m \hat{x}_{j,k}^{i-}$$

(d) State covariance error estimation

$$P_k^- = E\left[\left(\hat{x}_{j,k}^{i-} - \hat{x}_k^{i-}\right)\cdot\left(\hat{x}_{j,k}^{i-} - \hat{x}_k^{i-}\right)^T\right] + \left(\sum_{m=1}^{k} K_m \hat{x}_{k-m}^{i+}\right)^T E\left[\left(\hat{x}_{j,k}^{i-} - \hat{x}_k^{i-}\right)\right] + \left(\sum_{m=1}^{k} K_m \hat{x}_{k-m}^{i+}\right) E\left[\left(\hat{x}_{j,k}^{i-} - \hat{x}_k^{i-}\right)^T\right] + \sum_{m=1}^{k} K_m \hat{x}_{k-m}^{i+} \left(\hat{x}_{k-m}^{i+}\right)^T \left(K_m\right)^T + Q_{k-1}$$

Step 3: Measurement update

(a) Update sigma points

$$\left[\hat{x}_k^{i-} \quad \hat{x}_k^{i-} + \left(\sqrt{(n+\kappa)P_k^-}\right) \quad \hat{x}_k^{i-} - \left(\sqrt{(n+\kappa)P_k^-}\right)\right]$$

(b) Generate the measured value

$$\begin{cases} y_{j,k}^{i-} = h\left(\hat{x}_{j,k}^{i-}, u_k\right) \\ \hat{y}_k^{i-} = \sum_{j=0}^{2n} \omega_j^m y_{j,k}^{i-} \end{cases}$$

(c) Update covariance

$$P_{yy,k} = \sum_{j=0}^{2n} \omega_j^c \left[y_{j,k}^{i-} - \hat{y}_k^{i-} \right] \left[y_{j,k}^{i-} - \hat{y}_k^{i-} \right]^T + R_{k-1}$$

$$P_{xy,k} = \sum_{j=0}^{2n} \omega_j^c \left[x_{j,k}^{i-} - \hat{x}_k^{i-} \right] \left[y_{j,k}^{i-} - \hat{y}_k^{i-} \right]^T$$

Step 4: Update the posterior estimation and calculate the innovation

$$K_k = P_{xy,k} / P_{yy,k}$$

$$e_k = y_k - \hat{y}_k^{i-}$$

$$\hat{x}_k^{i+} = \hat{x}_k^{i-} + K e_k$$

$$P_k^+ = P_k^- - K P_{yy,k} K^T$$

Step 5: Adaptive noise calculation

(a) Calculate residual sequence and real-time estimation of the covariance matrix

$$\varepsilon_k = y_k - h\left(\hat{x}_k^{i+}, u_k \right)$$

$$H_k = \frac{1}{M} \sum_{i=k-M+1}^{k} \varepsilon_i \varepsilon_i^T$$

(b) Update the posterior sigma points

$$\left[\hat{x}_k^{i+} \quad \hat{x}_k^{i+} + \left(\sqrt{(n+\kappa) P_k^+} \right) \quad \hat{x}_k^{i+} - \left(\sqrt{(n+\kappa) P_k^+} \right) \right]$$

$$\begin{cases} y_{j,k}^{i+} = h\left(\hat{x}_{j,k}^{i+}, u_k \right) \\ \hat{y}_k^{i+} = \sum_{j=0}^{2n} \omega_j^m y_{j,k}^{i+} \end{cases}$$

$$P_{yy,k}^+ = \sum_{i=0}^{2n} \omega_i^c \left[y_{j,k}^{i+} - \hat{y}_k^{i+} \right] \left[y_{j,k}^{i+} - \hat{y}_k^{i+} \right]^T$$

(c) Adaptive noise update

$$R_k = H_k + P_{yy,k}^+$$

$$Q_k = K H_k K^T$$

Step 6: Importance sampling: $\tilde{x}_k^{i+} \quad N(\hat{x}_k^{i+}, P_k^+)$

Step 7: Weight calculation and normalization

$$w_k^i = p(y_k \mid \tilde{x}_k^{i+}) = \frac{1}{\sqrt{2\pi R}} e^{\frac{-\left[y_k - h\left(\tilde{x}_k^{i+}, u_k \right) - w_k \right]^2}{2R}}$$

$$w_k^i = w_k^i / \sum_{i=1}^{M} w_k^i$$

Step 8: Update estimates

$$\hat{x}_k^+ = \sum_{i=1}^{N} \tilde{x}_k^{i+} \omega_k^i$$

$$P_k = \sum_{i=1}^{M} w_k^i (\tilde{x}_k^{i+} - \hat{x}_k^+)(\tilde{x}_k^{i+} - \hat{x}_k^+)^T$$

3.3 A combined estimator of online full-parameter identification and SOC estimation

Since the battery model parameters will change with the change of the SOC, the combined estimator based on the model parameters and SOC has higher accuracy. However, combined estimators based on FOM are rarely implemented. Besides, the influence of non-Gaussian noise in the real environment must be considered. Based on the aforementioned full-parameter identification and the derivation of AFOUPF algorithm, the combined estimator can be applied to SOC estimation. This method ensures the high accuracy of the SOC in the whole cycle, and the adaptive algorithm is based on the residual sequence to overcome the divergence problem that may occur in the filtering process, which improves the adaptability of the algorithm. The implementation flow chart of full-parameter identification and SOC combined estimator is shown in Fig. 4.

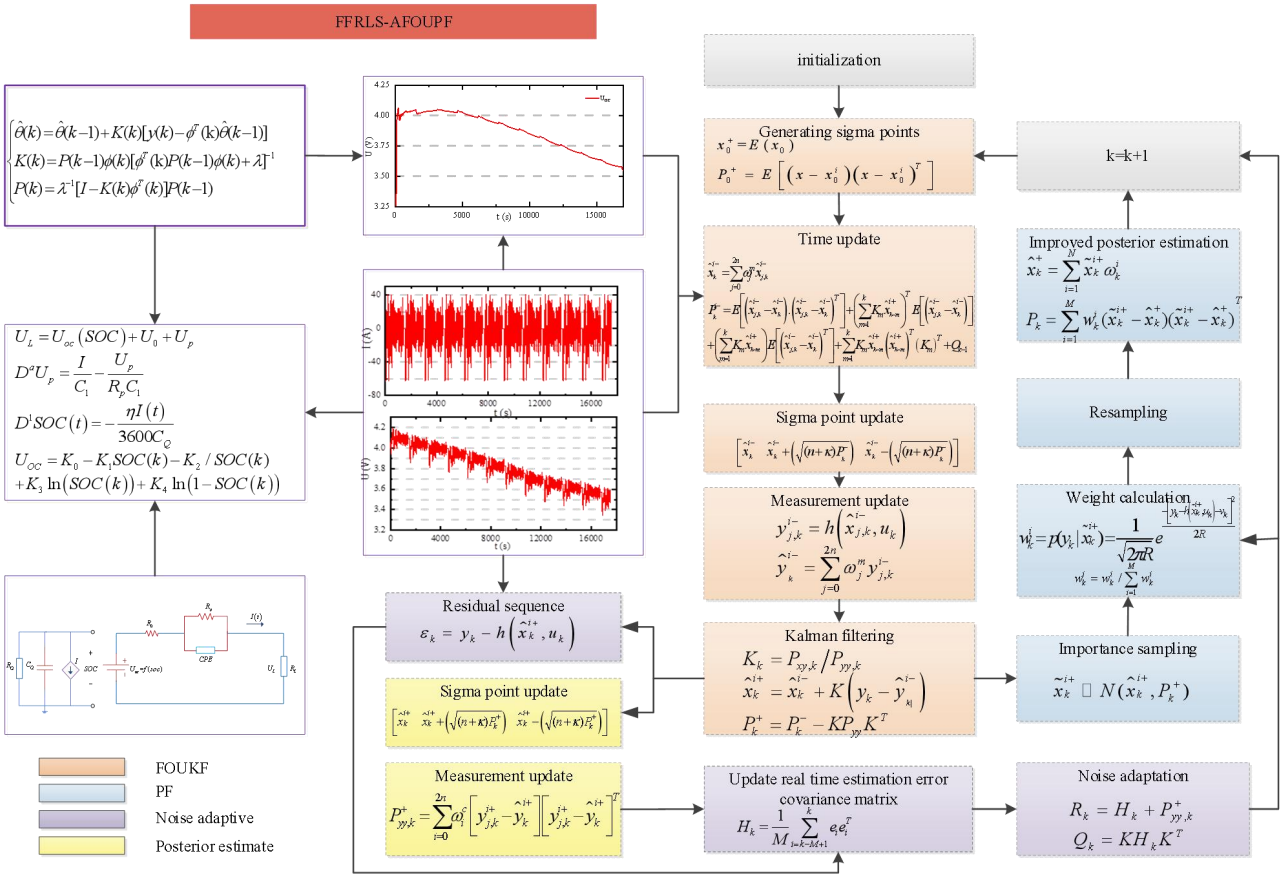

Fig 4 The combined estimator of full-parameter identification and SOC

The whole process consists of three parts. The first part is to realize the online full-parameters identification. The second part introduces the fractional-order theory and uses the AFOUKF algorithm to generate the probability density distribution of the PF algorithm. Finally, the closed-loop feedback of SOC estimation and

parameter identification is realized. Thus, the adaptive update of model parameters and SOC is realized, which ensures the convergence speed and accuracy of the algorithm.

4. Experimental analysis

4.1. Experimental working conditions

To verify the accuracy of the battery model and algorithm, the LiFePO4 battery is selected as the experimental object. The experimental equipment includes battery test equipment (CT-4016-5V100A-NTFA) for voltammetry measurements, a temperature chamber (DGBELL BTT-331C) for temperature control and a host computer for data recording. The entire battery test bench is as shown in Fig. 5.

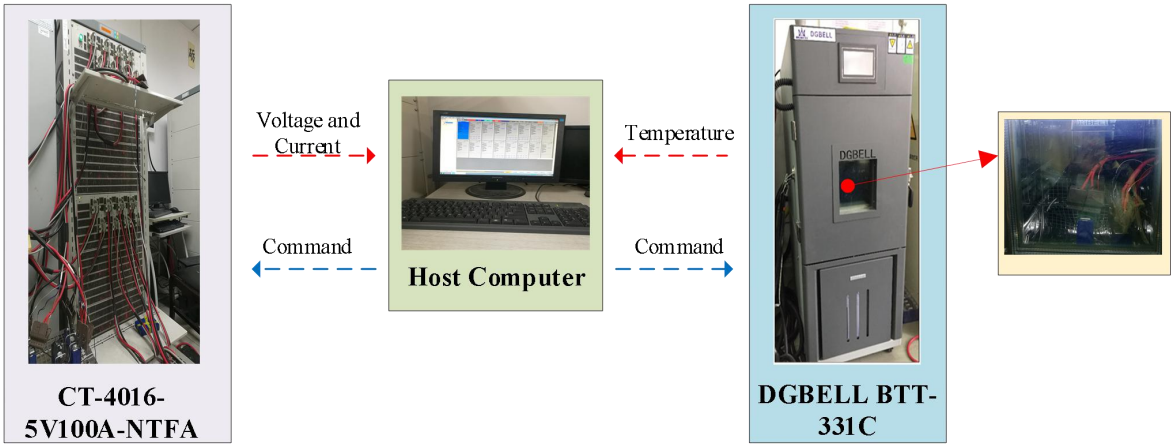

Fig. 5 The entire battery test bench

The urban dynamometer driving schedule (UDDS) profile is used to verify the reliability and accuracy of the proposed SOC estimation method, as shown in Fig. 6. Fig.6 (a) and (b) are the current and voltage curves during the UDDS test.

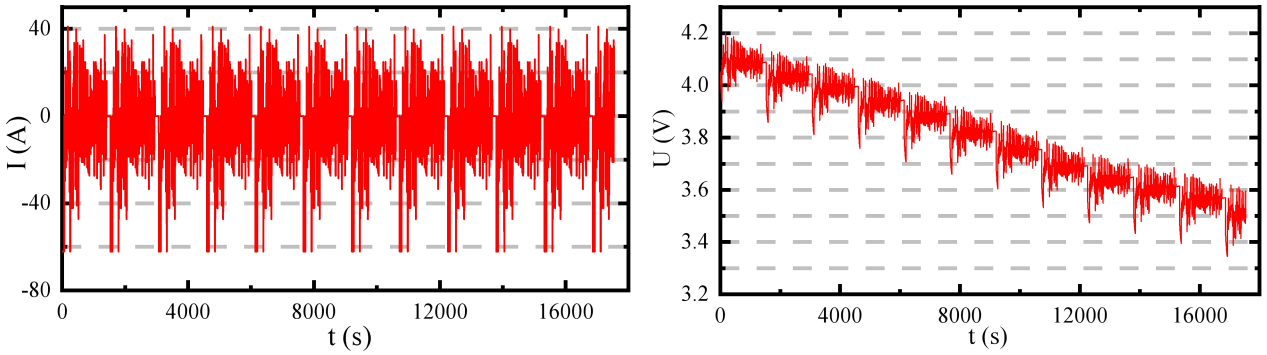

(a) Dynamic current profile (b) Voltage profiles

Fig. 6 Experimental data of UDDS condition

4.2. Parameter identification results

Based on the real-time current and voltage data recorded in the UDDS test experiment, the online full-parameter identification of FOM is carried out based on the FFRLS algorithm, and the identification results of open-circuit voltage, ohmic internal resistance, polarization internal resistance, and CPE are obtained, as shown in Fig 7.

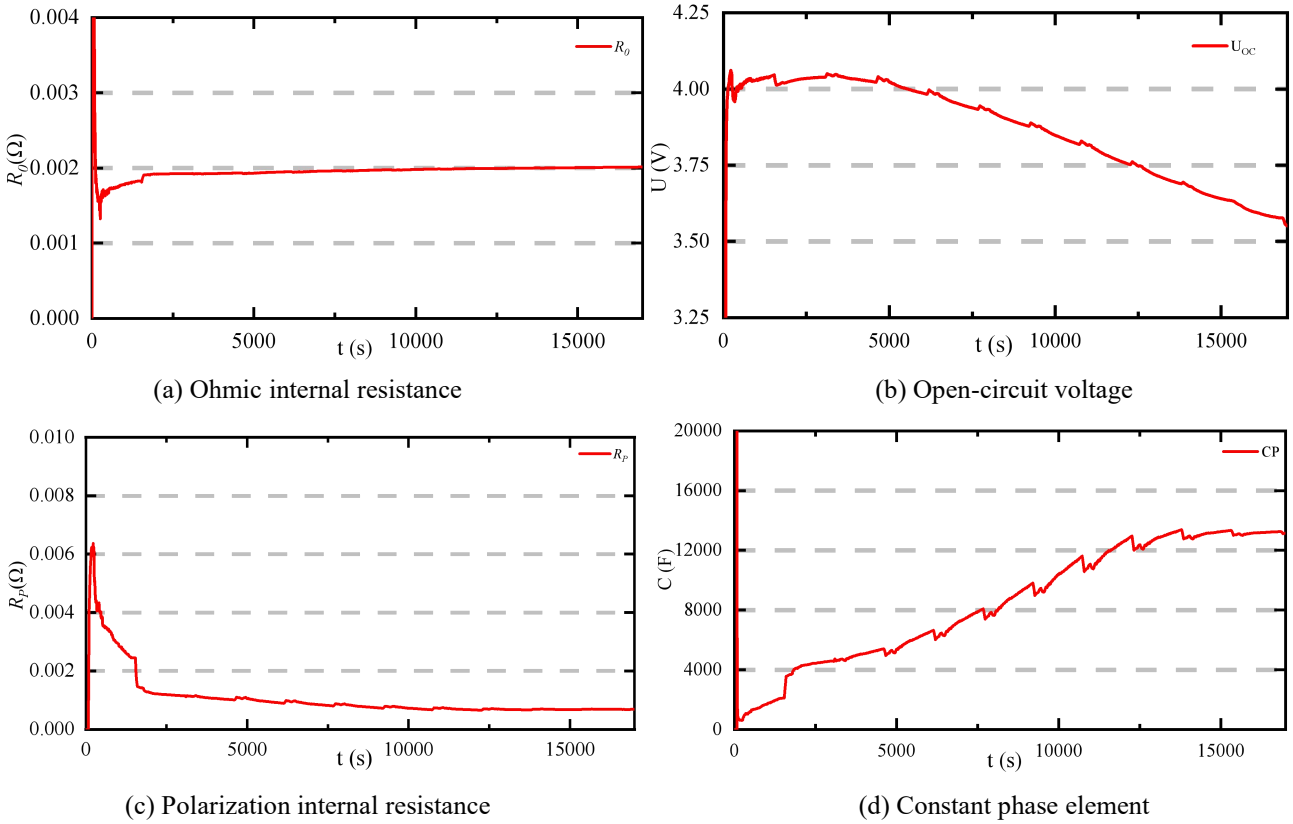

(a) Ohmic internal resistance (b) Open-circuit voltage

(c) Polarization internal resistance (d) Constant phase element

Fig 7 The full-parameter identification results

Fig.7 (a) shows that R_0 does not change much throughout the cycle. CPE and R_p tend to increase gradually. The main reason is that this component represents the effect of charge transfer and double-layer capacitance when the battery is working. When the SOC is small, the increase of li-ion concentration in the cathode hinders the subsequent li-ion insertion, which leads to an increase of resistance in the circuit. The coefficients of open-circuit voltage are shown in Tab 3.

Tab 3 The open-circuit voltage coefficients

K1	K2	K3	K4	K5
2.7800	-1.5611	0.0599	-0.4959	0.0368

4.3. SOC estimation results and verification

4.3.1. Model accuracy verification

To better reflect the accuracy of FOM and the convergence, accuracy, and robustness of the proposed method, IOM is chosen as the object of comparison and verification. The comparison between the model output voltage and the measured voltage is shown in Fig.8 (a), and the error between the model output voltage and the measured voltage is shown in Fig.8 (b).

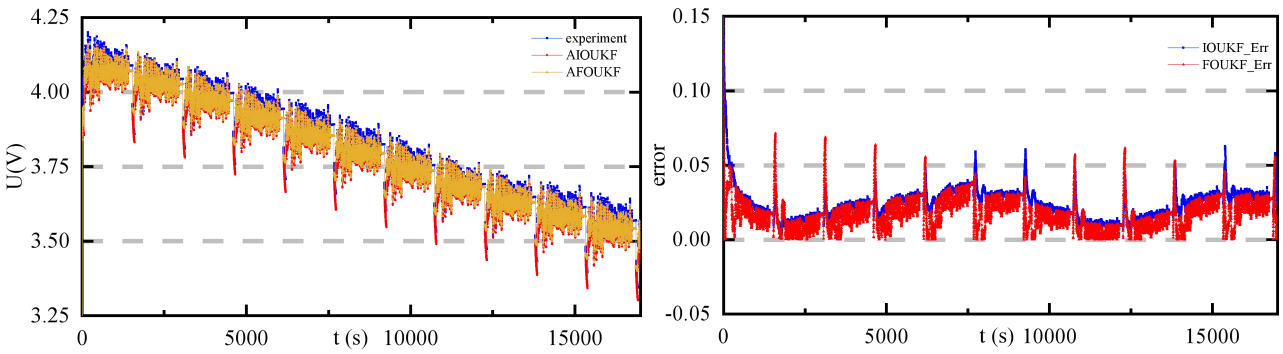

(a) Comparison voltage between the model output and the measured

(b) Error between the model output voltage and the measured voltage

Fig 8 Accuracy verification of UDDS

Fig 8 (a) shows that the fitting degree of the output voltage curve of the FOM and the measured voltage curve is very high, and the values are very close, indicating that the FOM parameter identification result is more accurate than the IOM. The RMSE is 0.02, and the error between the model voltage and the measured voltage does not exceed 0.05 V, and the error is relatively large only when the voltage and current change suddenly.

4.3.2. Performance comparison of different SOC estimation methods

To verify the accuracy and reliability of the algorithm, various methods have been selected to further verify the advantages of the method. The experiment solved the particle degradation problem in the PF algorithm by increasing the number of particles and selecting a reasonable probability density distribution.

The root mean square error (RMSE), mean absolute error (MAE), and mean absolute percentage error (MAPE) are selected to evaluate the model and state estimation results. The comparison results are shown in Tab 4.

Tab.4 Performance comparison of four algorithms under different sample particle numbers

evaluation index	Performance comparison of sample particle numbers and modeling methods				Performance comparison of sample particle numbers and probability density distribution			
	M=100		M=110		M=20		M=50	
	IOPF	FOPF	IOPF	FOPF	IOUPF	FOUPF	IOUPF	FOUPF
RMSE(%)	1.45	1.26	1.35	1.15	1.16	0.86	1.01	0.64
MAPE(%)	2.95	2.45	2.56	2.36	1.66	0.99	1.67	1.00
MAE(%)	1.15	0.95	1.03	0.89	0.66	0.4	0.68	0.4

Under the same estimation method, increasing the number of particles can improve the accuracy of SOC estimation. For both PF and UPF algorithms, the accuracy of FOM is higher than that of IOM under the same particle number, which shows the superiority of FOM. The estimation comparison based on four algorithms is shown in Fig.9.

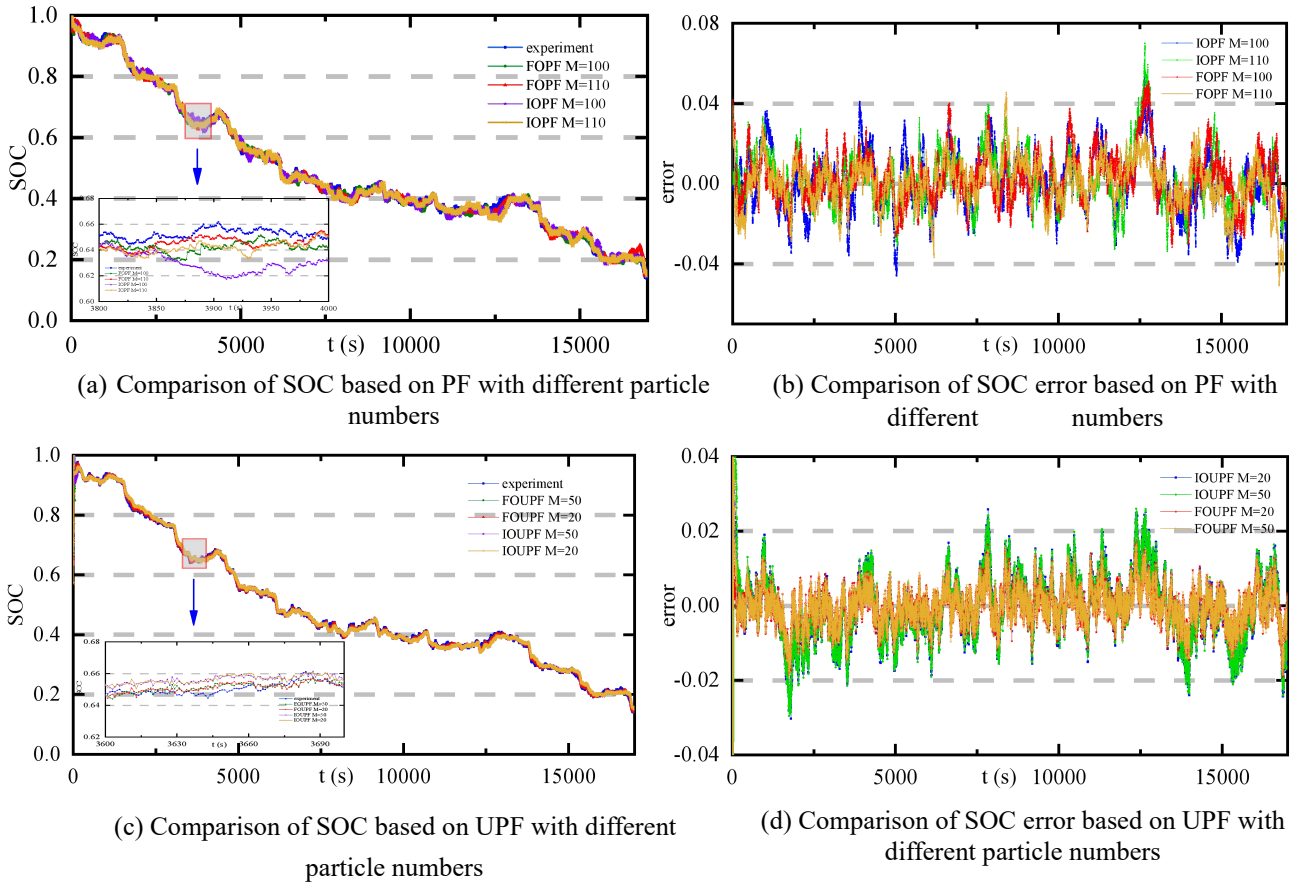

(a) Comparison of SOC based on PF with different particle numbers

(b) Comparison of SOC error based on PF with different numbers

(c) Comparison of SOC based on UPF with different particle numbers

(d) Comparison of SOC error based on UPF with different particle numbers

Fig 9 SOC estimation comparison based on four algorithms

Fig 9 shows that the four algorithms can accurately track changes in SOC, and the FOUPF algorithm has higher accuracy. When FOUPF has an initial error, the error will stabilize after a period of adaptive adjustment, which proves that the algorithm can be applied to actual complex working conditions. Since the FOUPF algorithm integrates the fractional-order theory and considers the past L input and output information of the system, the result is more accurate. At the same time, the introduction of differential order parameters as hidden parameters improves the UPF algorithm, which reduces the number of particles and running time while ensuring estimation accuracy.

Fig 9 shows the SOC estimation result based on offline parameter identification combined with FOUPF. To further verify the accuracy and superiority of the algorithm combining online full-parameter identification with AFOUPF, the following experimental verification is carried out.

4.3.3. SOC estimation results of online full-parameter identification based on unscented particle filter

The algorithm improves the suboptimal density function of the PF algorithm by fusing FOUKF, and adds the noise adaptive algorithm, which effectively suppresses the noise in the battery estimation process, improves the accuracy and reduces the impact of noise. The online full-parameter identification and the SOC combined estimator promote the improvement of battery SOC estimation accuracy, and the real-time update of the SOC value makes all parameters have higher accuracy throughout the cycle. Fig.10 shows the SOC comparison

results of the two algorithms when M=20.

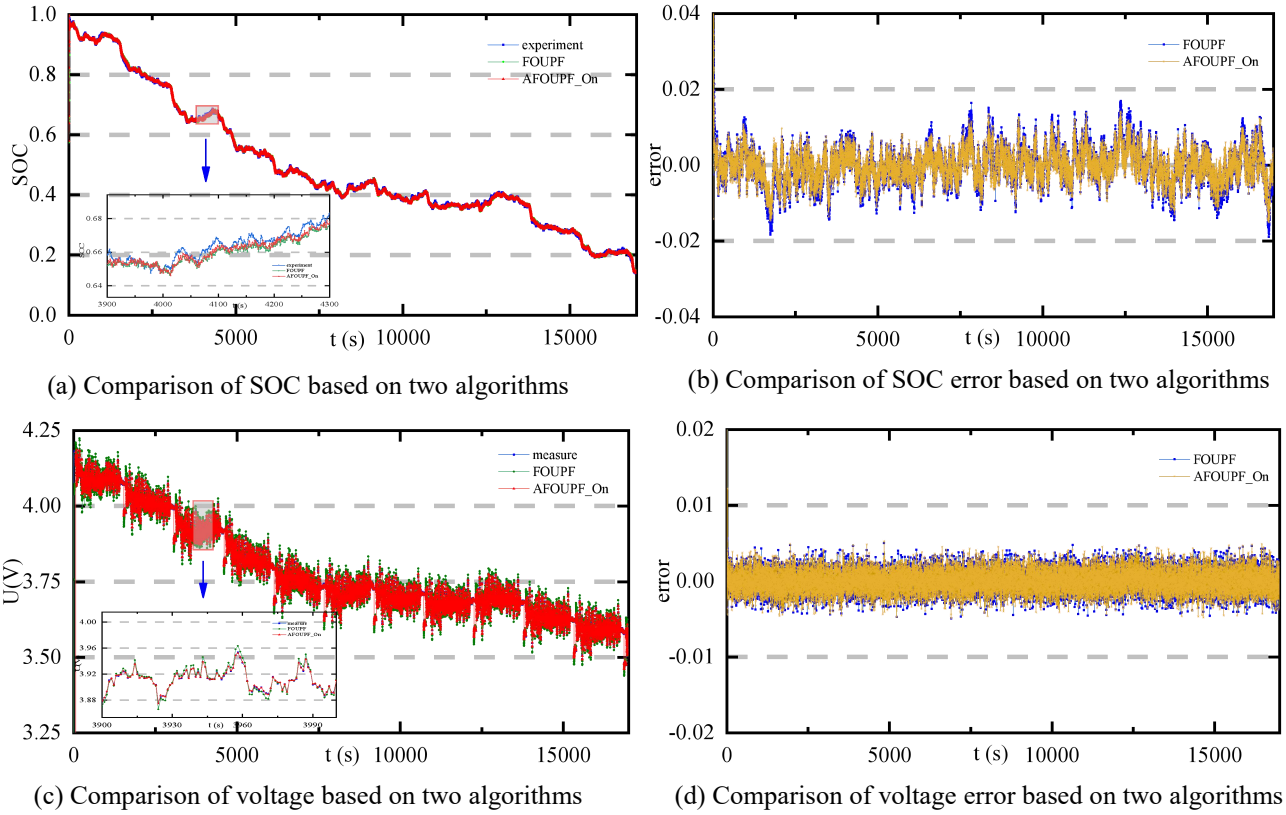

(a) Comparison of SOC based on two algorithms

(b) Comparison of SOC error based on two algorithms

(c) Comparison of voltage based on two algorithms

(d) Comparison of voltage error based on two algorithms

Fig 10 Performance comparison based on two algorithms

Fig 10 shows that both algorithms can track changes in SOC very well, indicating the correctness of the algorithm applied to SOC estimation. Even if the error is large at the beginning and end of the cycle, the algorithm based on online full-parameter identification has better tracking effect and higher estimation accuracy in the whole cycle. The results show that the adaptive update of model parameters and SOC can significantly reduce the SOC estimation error and obtain higher estimation accuracy.

The RMSE of the algorithm is 0.67%, the MAPE and the MAE are 0.82%, 0.33% respectively, and the performance evaluation index is better than that in [41] and [30]. In ref.[41], the average error of the AFOEKF algorithm is 1.37%, which is lower than that of FOEKF and AIOEKF algorithms under the same conditions, indicating the necessity of FOM and noise adaptive algorithms. In ref [30], Wang et al proposed a method of estimating SOC by combining the particle filter and the fractional Kalman filter. Set M=500, which will lead to higher computational complexity. The experimental results show that the estimation error is less than 1% under the condition of constant current, and less than 4% under the condition of variable current.

Therefore, the combined algorithm proves that the adaptive adjustment of the process noise covariance and the observation noise covariance can significantly improve SOC estimation results. The results show that the MAE, RMSE, and MAPE of the SOC obtained by the combined estimation algorithm are the smallest, indicating that the online full-parameters identification is required to improve the accuracy of SOC estimation results.

5. Conclusions

A combined estimator of online full-parameter identification and adaptive unscented particle filter for Li-ion battery SOC is proposed based on an improved fractional-order model. Firstly, the iterative complexity of the algorithm is reduced by reducing the number of particles. Secondly, the adaptive algorithm based on residual sequence can solve the divergence problem and improve the adaptability of the algorithm. At the same time, online full-parameter identification can solve the problem of the large estimation error of traditional algorithm in low SOC intervals and high SOC intervals, and overcome the shortcomings of long cumulative error and long experimental time. Finally, the closed-loop feedback of SOC estimation and parameter identification is realized, which ensures the convergence speed and accuracy of the algorithm. The experimental results show that the evaluation index of the algorithm is the best, RMSE is 0.67%, and the SOC estimation is more accurate. It is shown that the algorithm has strong robustness and fast convergence. It should be noted that the ambient temperature on estimation performance will be a necessary study, which can be considered as our future work.

6. Acknowledgments

The work is supported by the National Natural Science Foundation of China (No. 61801407), Sichuan science and technology program (No. 2019YFG0427), China Scholarship Council (No. 201908515099), and Fund of Robot Technology Used for Special Environment Key Laboratory of Sichuan Province (No. 18kftk03).

Reference

1. Zou, C., et al., *A review of fractional-order techniques applied to lithium-ion batteries, lead-acid batteries, and supercapacitors.* Journal of Power Sources, 2018. **390**: p. 286-296.
2. Sun, T., et al., *A Novel Hybrid Prognostic Approach for Remaining Useful Life Estimation of Lithium-Ion Batteries.* Energies, 2019. **12**(19).
3. Wang, Y., et al., *A comprehensive review of battery modeling and state estimation approaches for advanced battery management systems.* Renewable & Sustainable Energy Reviews, 2020. **131**.
4. Wang, Q., et al., *A novel consistency evaluation method for series-connected battery systems based on real-world operation data.* IEEE Transactions on Transportation Electrification, 2020: p. 1-1.
5. Zhang, L., et al., *Battery heating for lithium-ion batteries based on multi-stage alternative currents.* Journal of Energy Storage, 2020. **32**: p. 101885.
6. She, C., et al., *Battery Aging Assessment for Real-World Electric Buses Based on Incremental Capacity Analysis and Radial Basis Function Neural Network.* IEEE Transactions on Industrial Informatics, 2020. **16**(5): p. 3345-3354.
7. Zhang, K., et al., *State of Charge Estimation for Lithium Battery Based on Adaptively Weighting Cubature Particle Filter.* Ieee Access, 2019. **7**: p. 166657-166666.
8. Jiang, C., et al., *A state-of-charge estimation method of the power lithium-ion battery in complex conditions based on adaptive square root extended Kalman filter.* Energy, 2021. **219**: p. 119603.
9. Nasser-Eddine, A., et al., *A two steps method for electrochemical impedance modeling using fractional order system in time and frequency domains.* Control Engineering Practice, 2019. **86**: p. 96-104.
10. Zhang, Q., et al., *A novel fractional variable-order equivalent circuit model and parameter identification of*

electric vehicle Li-ion batteries. ISA Trans, 2020. **97**: p. 448-457.
11. Wang, Y., et al., *A fractional-order model-based state estimation approach for lithium-ion battery and ultra-capacitor hybrid power source system considering load trajectory.* Journal of Power Sources, 2020. **449**: p. 227543.
12. Zhang, Q., et al., *A Fractional-Order Kinetic Battery Model of Lithium-Ion Batteries Considering a Nonlinear Capacity.* Electronics, 2019. **8**(4).
13. Hu, M., et al., *Lithium-ion battery modeling and parameter identification based on fractional theory.* Energy, 2018. **165**: p. 153-163.
14. Jin, G., et al., *Comparison of SOC Estimation between the Integer-Order Model and Fractional-Order Model Under Different Operating Conditions.* Energies, 2020. **13**(7).
15. Huai, R., Z. Yu, and H. Li, *Historical data demand in window-based battery parameter identification algorithm.* Journal of Power Sources, 2019. **433**.
16. De Sutter, L., et al., *Battery aging assessment and parametric study of lithium-ion batteries by means of a fractional differential model.* Electrochimica Acta, 2019. **305**: p. 24-36.
17. Xu, Y., et al., *State of charge estimation for lithium-ion batteries based on adaptive dual Kalman filter.* Applied Mathematical Modelling, 2020. **77**: p. 1255-1272.
18. Tian, J., et al., *A Comparative Study of Fractional Order Models on State of Charge Estimation for Lithium Ion Batteries.* Chinese Journal of Mechanical Engineering, 2020. **33**(1).
19. Chen, Y., et al., *A New State of Charge Estimation Algorithm for Lithium-Ion Batteries Based on the Fractional Unscented Kalman Filter.* Energies, 2017. **10**(9): p. 1313.
20. Li, X., Z. Wang, and L. Zhang, *Co-estimation of capacity and state-of-charge for lithium-ion batteries in electric vehicles.* Energy, 2019. **174**: p. 33-44.
21. Xia, B., et al., *A State of Charge Estimation Method Based on Adaptive Extended Kalman-Particle Filtering for Lithium-ion Batteries.* Energies, 2018. **11**(10).
22. Xiong, R., et al., *A Novel Fractional Order Model for State of Charge Estimation in Lithium Ion Batteries.* Ieee Transactions on Vehicular Technology, 2019. **68**(5): p. 4130-4139.
23. Xie, G., et al., *Remaining useful life prediction of lithium-ion battery based on an improved particle filter algorithm.* Canadian Journal of Chemical Engineering, 2019.
24. Li, B., K. Peng, and G. Li, *State-of-charge estimation for lithium-ion battery using the Gauss-Hermite particle filter technique.* Journal of Renewable and Sustainable Energy, 2018. **10**(1).
25. Liu, X., et al., *An Improved State of Charge and State of Power Estimation Method Based on Genetic Particle Filter for Lithium-ion Batteries.* Energies, 2020. **13**(2).
26. Wang, L. and R. Ding, *A parameter determination method of unscented transformation and its approximate ability analysis in the precision estimation of nonlinear measurement adjustment.* Measurement, 2020. **166**: p. 108065.
27. Tian, J., et al., *Online simultaneous identification of parameters and order of a fractional order battery model.* Journal of Cleaner Production, 2020. **247**.
28. Wang, Y. and Z. Chen, *A framework for state-of-charge and remaining discharge time prediction using unscented particle filter.* Applied Energy, 2020. **260**: p. 114324.
29. Li, S., et al., *Adaptive state of charge estimation for lithium-ion batteries based on implementable fractional-order technology.* Journal of Energy Storage, 2020. **32**: p. 101838.
30. Wang, J., et al., *Fractional Order Equivalent Circuit Model and SOC Estimation of Supercapacitors for Use in HESS.* IEEE Access, 2019. **7**: p. 52565-52572.
31. Li, S., et al., *Fractional-order modeling and SOC estimation of lithium-ion battery considering capacity loss.* International Journal of Energy Research, 2019. **43**(1): p. 417-429.
32. Tian, J., et al., *Fractional order battery modelling methodologies for electric vehicle applications: Recent advances and perspectives.* Science China-Technological Sciences, 2020.

33. Tian, J., R. Xiong, and Q. Yu, *Fractional-Order Model-Based Incremental Capacity Analysis for Degradation State Recognition of Lithium-Ion Batteries.* Ieee Transactions on Industrial Electronics, 2019. **66**(2): p. 1576-1584.
34. Li, L., et al., *A Novel Online Parameter Identification Algorithm for Fractional-Order Equivalent Circuit Model of Lithium-Ion Batteries.* International Journal of Electrochemical Science, 2020. **15**(7): p. 6863-6879.
35. Lai, X., et al., *Co-estimation of state of charge and state of power for lithium-ion batteries based on fractional variable-order model.* Journal of Cleaner Production, 2020. **255**.
36. Sierociuk, D., et al., *Dual Estimation of Fractional Variable Order Based on the Unscented Fractional Order Kalman Filter for Direct and Networked Measurements.* Circuits, Systems, and Signal Processing, 2016. **35**(6): p. 2055-2082.
37. Ramezani, A. and B. Safarinejadian, *A Modified Fractional-Order Unscented Kalman Filter for Nonlinear Fractional-Order Systems.* Circuits, Systems, and Signal Processing, 2017. **37**(9): p. 3756-3784.
38. Tian, J., et al., *Frequency and time domain modelling and online state of charge monitoring for ultracapacitors.* Energy, 2019. **176**: p. 874-887.
39. Chen, X., et al., *Hybrid extended-unscented Kalman filters for continuous-time nonlinear fractional-order systems involving process and measurement noises.* Transactions of the Institute of Measurement and Control, 2020. **42**(9): p. 1618-1631.
40. Gao, Z., et al., *Unscented Kalman filter for continuous‐time nonlinear fractional‐order systems with process and measurement noises.* Asian Journal of Control, 2019. **22**(5): p. 1961-1972.
41. Zhu, Q., et al., *A state of charge estimation method for lithium-ion batteries based on fractional order adaptive extended kalman filter.* Energy, 2019. **187**.

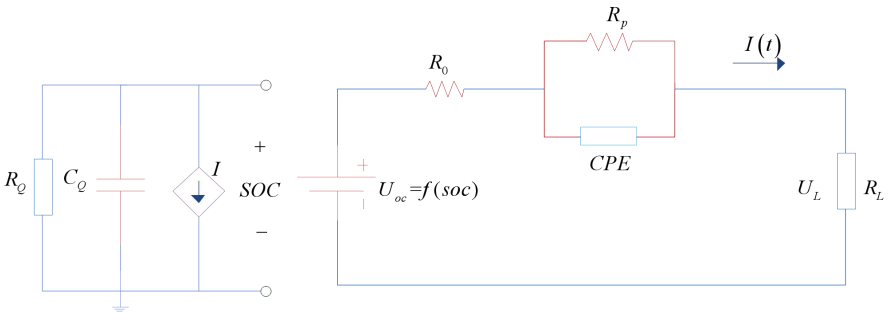

Fig1. Runtime-based fractional-order battery model

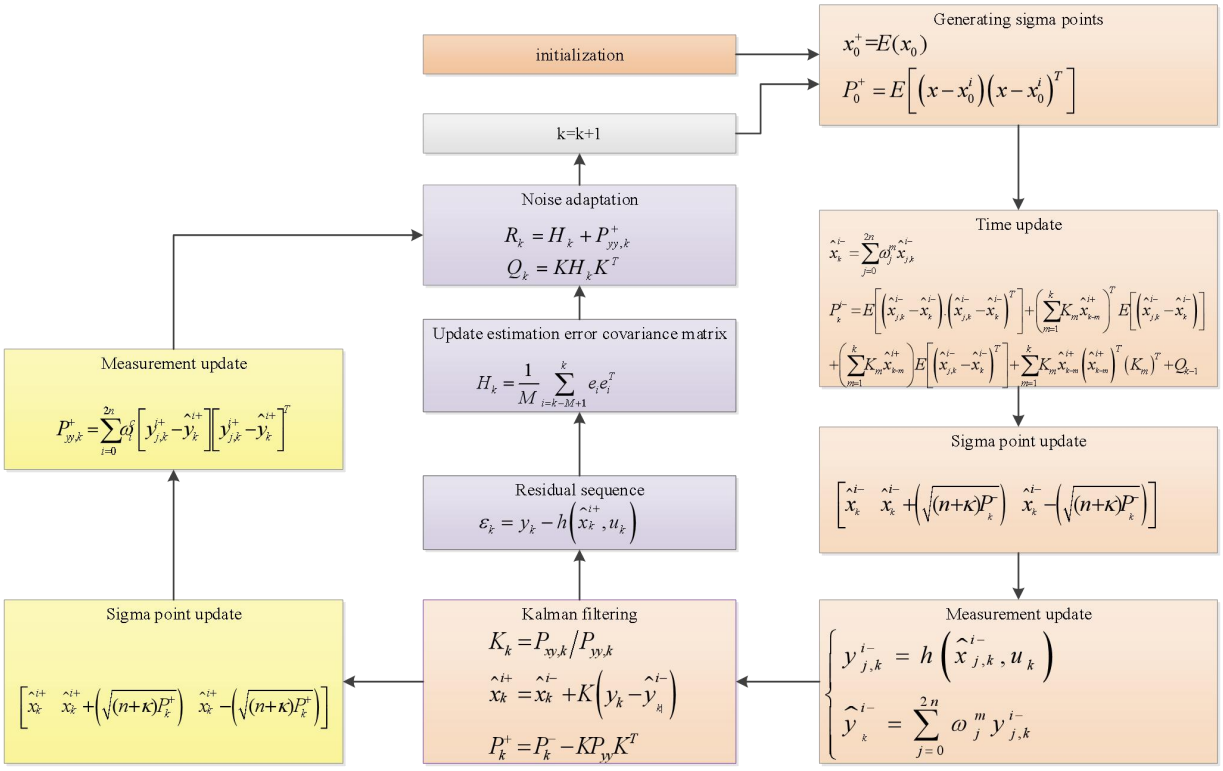

Fig 2 The flow chart of SOC estimation based on residual sequence adaptive fractional-order unscented Kalman filter

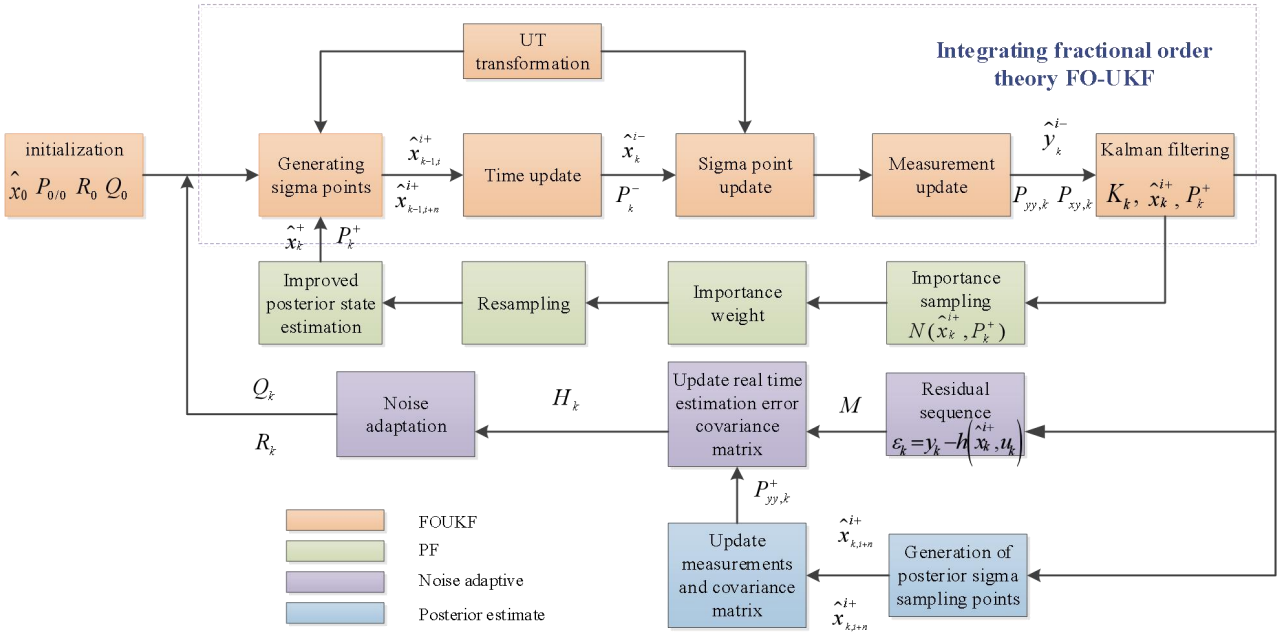

Fig 3 The flow chart of the adaptive fractional-order unscented particle filter algorithm

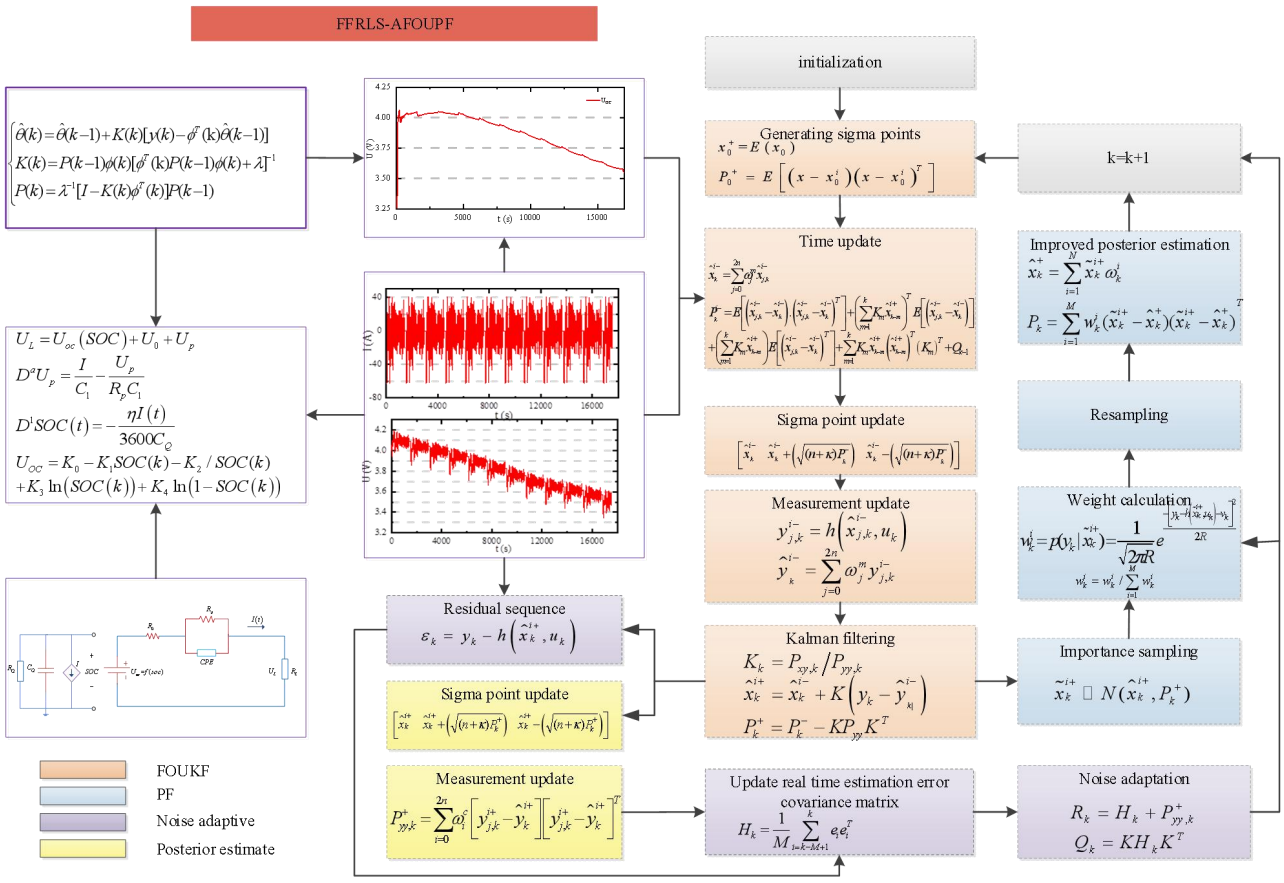

Fig 4 The combined estimator of full-parameter identification and SOC

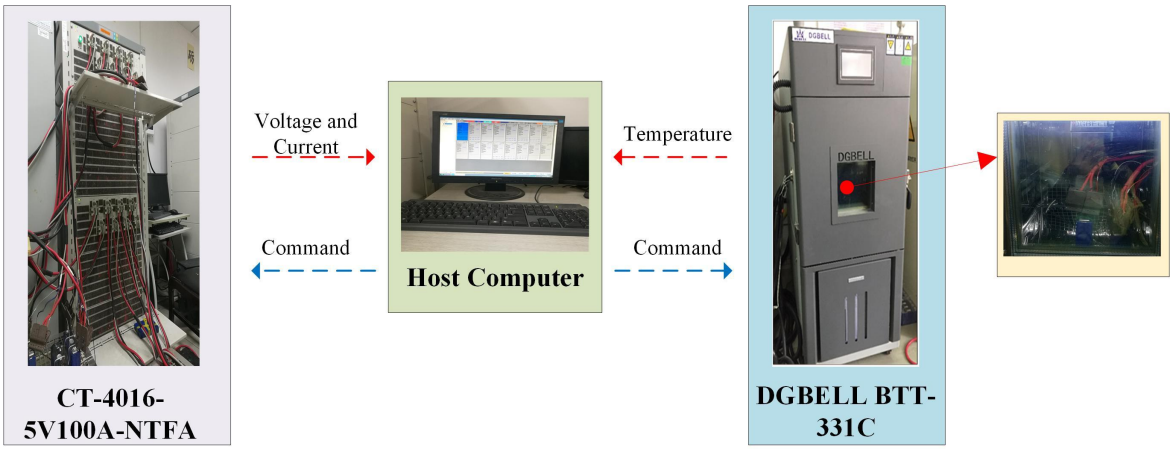

Fig. 5 The entire battery test bench

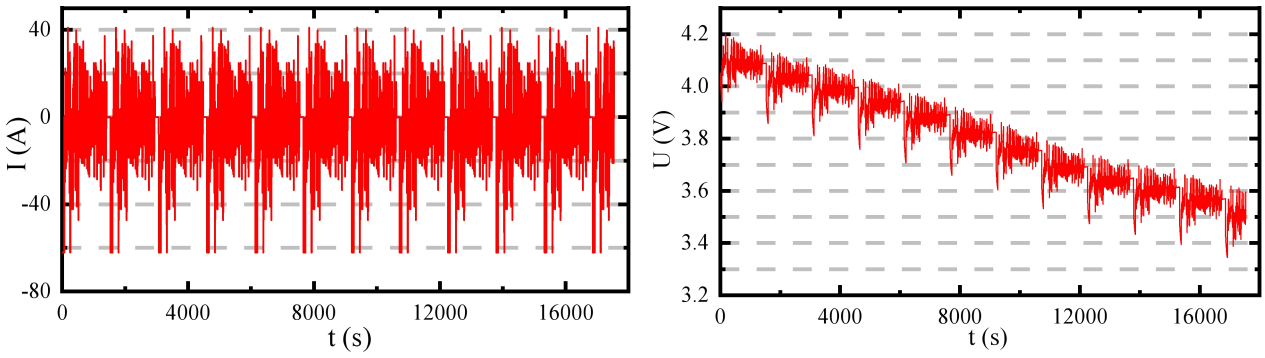

(a) Dynamic current profile (b) Voltage profiles

Fig. 6 Experimental data of UDDS condition

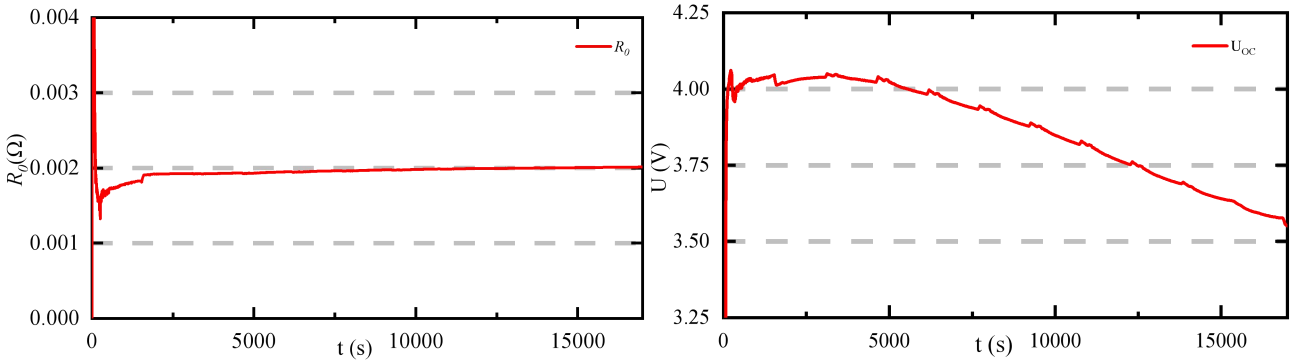

(a) Ohmic internal resistance (b) Open-circuit voltage

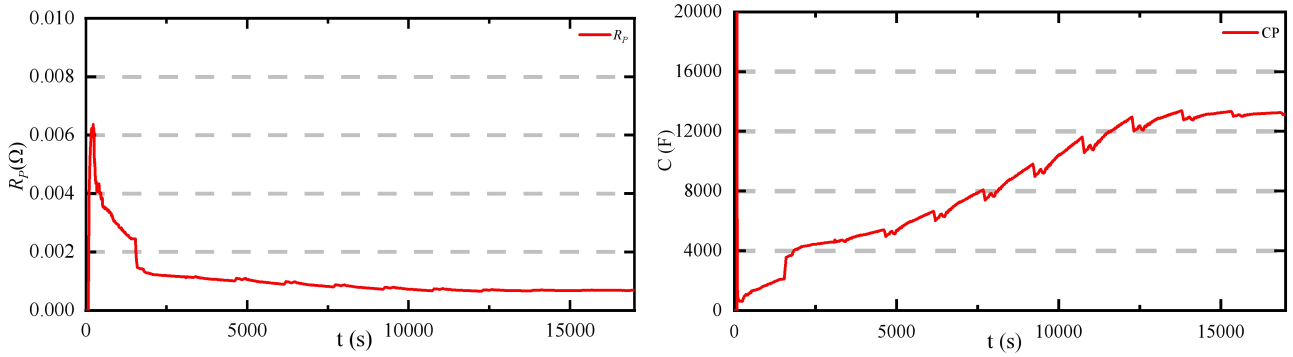

(c) Polarization internal resistance (d) Constant phase element

Fig 7 The full-parameter identification results

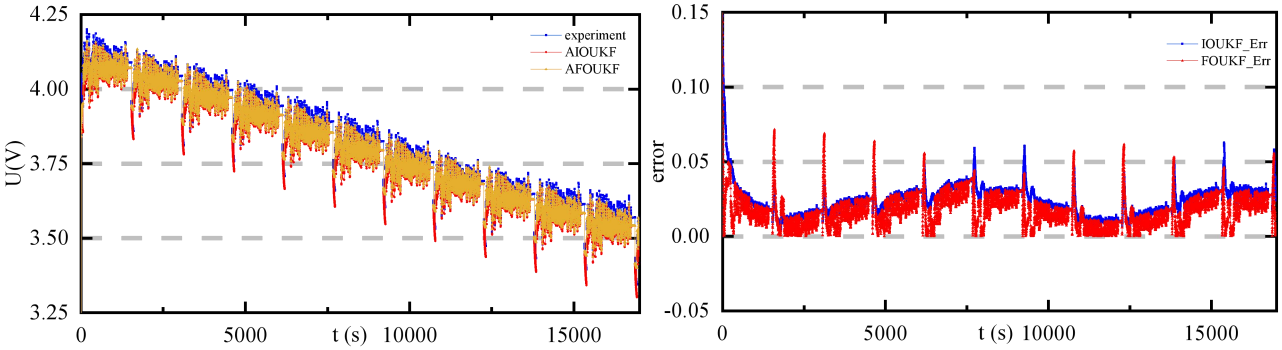

(a) Comparison voltage between the model output and the measured (b) Error between the model output voltage and the measured voltage

Fig 8 Accuracy verification of UDDS

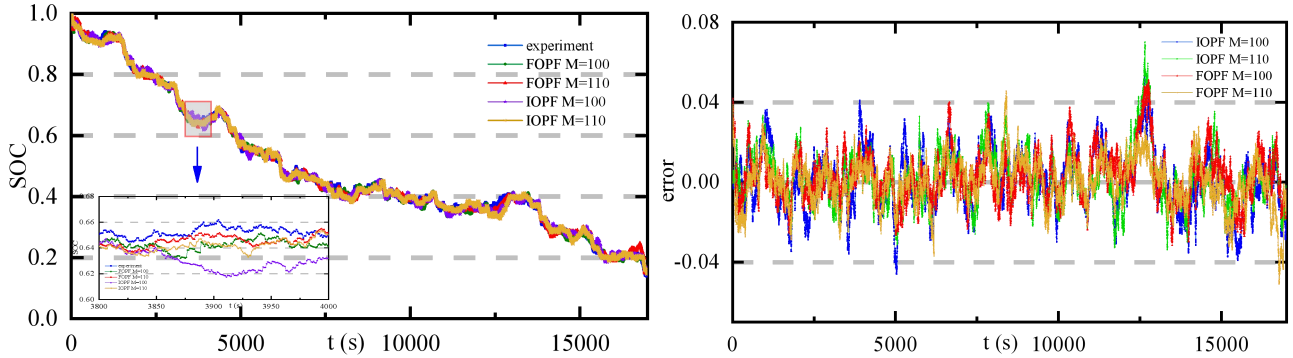

(a) Comparison of SOC based on PF with different particle numbers (b) Comparison of SOC error based on PF with different particle numbers

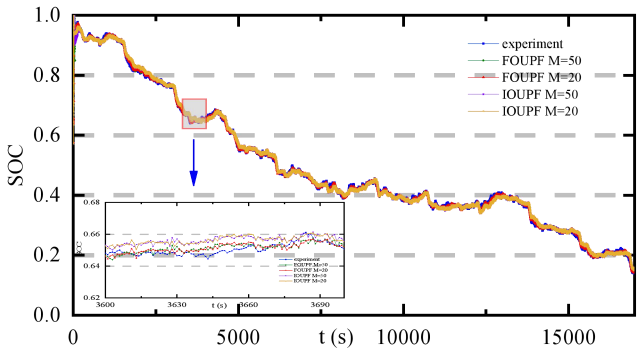

(c) Comparison of SOC based on UPF with different particle numbers

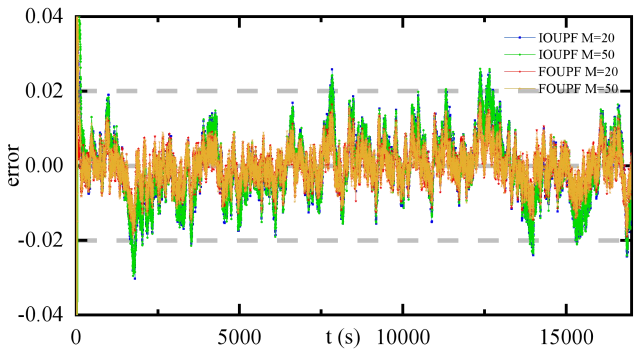

(d) Comparison of SOC error based on UPF with different particle numbers

Fig 9 SOC estimation comparison based on four algorithms

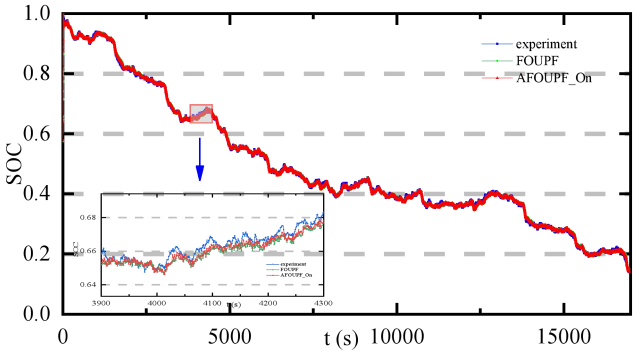

(a) Comparison of SOC based on two algorithms

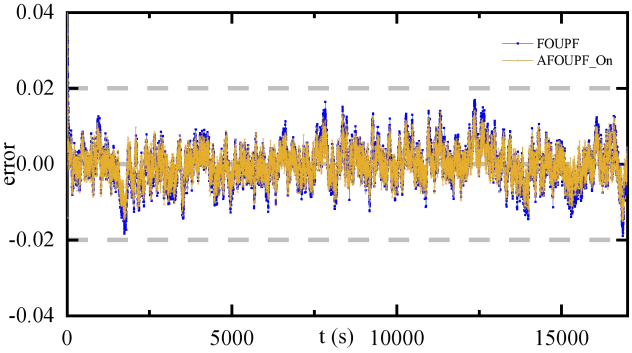

(b) Comparison of SOC error based on two algorithms

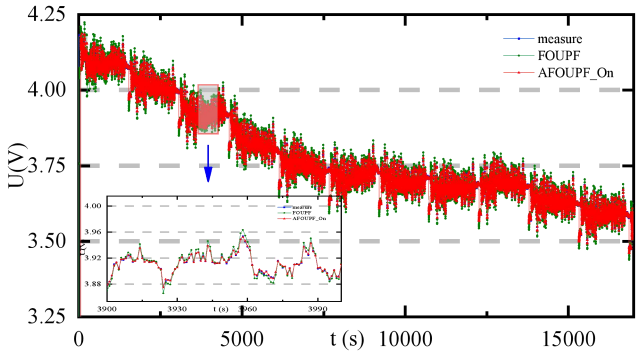

(c) Comparison of voltage based on two algorithms

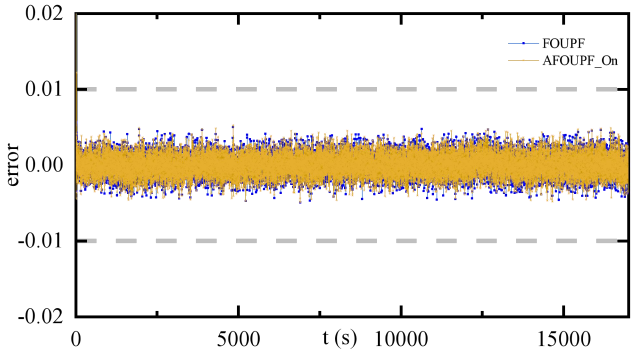

(d) Comparison of voltage error based on two algorithms

Fig 10 Performance comparison based on two algorithms